© 2023. Published by The Company of Biologists Ltd | Development (2023) 150, dev201959. doi:10.1242/dev.201959

RESEARCH ARTICLE

ARRDC5 deficiency impairs spermatogenesis by affecting SUN5 and NDC1

Ruyi Liu[1,*], Ronggui Qu[1,*], Qun Li[1], Biaobang Chen[2], Jian Mu[1], Yang Zeng[1], Yuxi Luo[1], Fangzhou Xu[1], Lei Wang[1,‡], Zhihua Zhang[1,‡] and Qing Sang[1,‡]

ABSTRACT

Sperm with normal morphology and motility are essential for successful fertilization, and the strong attachment of the sperm head-tail coupling apparatus to the nuclear envelope during spermatogenesis is required to ensure the integrity of sperm for capacitation and fertilization. Here, we report that *Arrdc5* is associated with spermatogenesis. The *Arrdc5* knockout mouse model showed male infertility characterized by a high bent-head rate and reduced motility in sperm, which led to capacitation defects and subsequent fertilization failure. Through mass spectrometry, we found that ARRDC5 affects spermatogenesis by affecting NDC1 and SUN5. We further found that ARRDC5 might affect the vesicle-trafficking protein SEC22A-mediated transport and localization of NDC1, SUN5 and other head-tail coupling apparatus-related proteins that are responsible for initiating the attachment of the sperm head and tail. We finally performed intracytoplasmic sperm injection as a way to explore therapeutic strategies. Our findings demonstrate the essential role and the underlying molecular mechanism of ARRDC5 in anchoring the sperm head to the tail during spermatogenesis.

KEY WORDS: ARRDC5, Spermatogenesis, Sperm head–tail coupling apparatus, Male infertility

INTRODUCTION

Sperm are highly specialized cells that deliver DNA of the male parent to the offspring; sperm with normal morphology and mobility are crucial for successful fertilization. Mammalian sperm are produced by the complex and precisely orchestrated process of spermatogenesis in the testis, which can be divided into the following three steps: the division of diploid spermatogonia, the formation of haploid round spermatids and morphogenetic transformation events for sperm formation. Morphogenetic transformation events (also called spermiogenesis) include nucleus condensation and elongation, acrosome biogenesis, flagellum formation and cytoplasm removal (Hao et al., 2019; Tanaka and Baba, 2005). Any defects during these processes may lead to azoospermia, to teratozoospermia or to sperm morphology and function defects, all of which can result in male infertility.

The arrestin family of proteins, including visual arrestins and β-arrestins, were originally identified as binding to phosphorylated G protein-coupled receptors and causing their desensitization (Gurevich et al., 1995). A larger family of proteins called α-arrestins (also called arrestin-related trafficking adaptors) were subsequently reported to share the overall arrestin-fold structure. So far, six α-arrestins have been identified, all of them sharing arrestin-like domains, including arrestin domain-containing protein 1 (ARRDC1), ARRDC2, ARRDC3, ARRDC4, ARRDC5 and thioredoxin-interacting protein (TXNIP) (Alvarez, 2008). It has been reported that ARRDC4 is important for sperm maturation by controlling extracellular vesicles release (Foot et al., 2021), but the roles of the other α-arrestins in spermatogenesis and male infertility have remained unclear. According to the mouse ENCODE transcriptome data (Yue et al., 2014), ARRDC5 is different from other α-arrestins by being specifically highly expressed in the testis, which suggests a role in male fertility. Thus, in this study we aimed to explore the expression pattern of ARRDC5 and its physiological functions in spermatogenesis and male fertility. During the preparation of this article, a study reported the role of *Arrdc5* in sperm spermatogenesis (Giassetti et al., 2023). However, that study mainly performed a phenotypic analysis by using *Arrdc5* knockout mice, and the underlying molecular mechanisms and signaling pathways for how ARRDC5 affects spermatogenesis remain unclear.

Here, we report that ARRDC5 is essential for spermatogenesis. *Arrdc5* knockout mice showed male infertility with abnormal sperm morphology, reduced motility and failed capacitation. Through mass spectrometry of testis extracts, we found that ARRDC5 deficiency caused reduced SUN5 and NDC1 protein levels, which are essential for anchoring the sperm head to the tail. Furthermore, we found that ARRDC5 deficiency might affect the SEC22A-mediated transport and localization of SUN5 and NDC1, thus leading to spermatogenesis defects. In addition, we performed intracytoplasmic sperm injection (ICSI) and obtained blastocysts, which can be considered as a rescue therapeutic strategy. Our results reveal the previously unrecognized role of ARRDC5 in SUN5 and NDC1 transport and localization, and reveal a previously unreported signaling pathway involved in sperm head and tail anchoring.

RESULTS

Arrdc5$^{-/-}$ male mice are infertile with abnormal sperm morphology and motility

Arrdc5 is specifically highly expressed in the testicular tissue of mice (Fig. 1A), and to investigate the role of ARRDC5, we generated *Arrdc5* knockout mice using CRISPR/Cas-mediated genome engineering (Fig. 1B,C). A 4-month period of mating showed that *Arrdc5*$^{-/-}$ female mice and *Arrdc5*$^{+/+}$ and *Arrdc5*$^{+/-}$ male mice could generate offspring normally, whereas *Arrdc5*$^{-/-}$ male mice mating with wild-type female mice could not generate offspring

[1]Institute of Pediatrics, Children's Hospital of Fudan University, the Institutes of Biomedical Sciences, and the State Key Laboratory of Genetic Engineering, Fudan University, Shanghai 200032, China. [2]NHC Key Lab of Reproduction Regulation (Shanghai Institute for Biomedical and Pharmaceutical Technologies), Fudan University, Shanghai 200032, China.
*These authors contributed equally to this work

‡Authors for correspondence (wangleiwanglei@fudan.edu.cn; zhihuazhang16@fudan.edu.cn; sangqing@fudan.edu.cn)

R.L., 0000-0003-3863-3439; R.Q., 0000-0001-9528-180X; B.C., 0000-0002-9921-2155; J.M., 0000-0001-6923-6415; L.W., 0000-0002-3400-0434; Z.Z., 0000-0002-4725-883X; Q.S., 0000-0002-9895-1394

Handling Editor: Swathi Arur
Received 8 May 2023; Accepted 17 November 2023

Development (2023) 150, dev201959. doi:10.1242/dev.201959

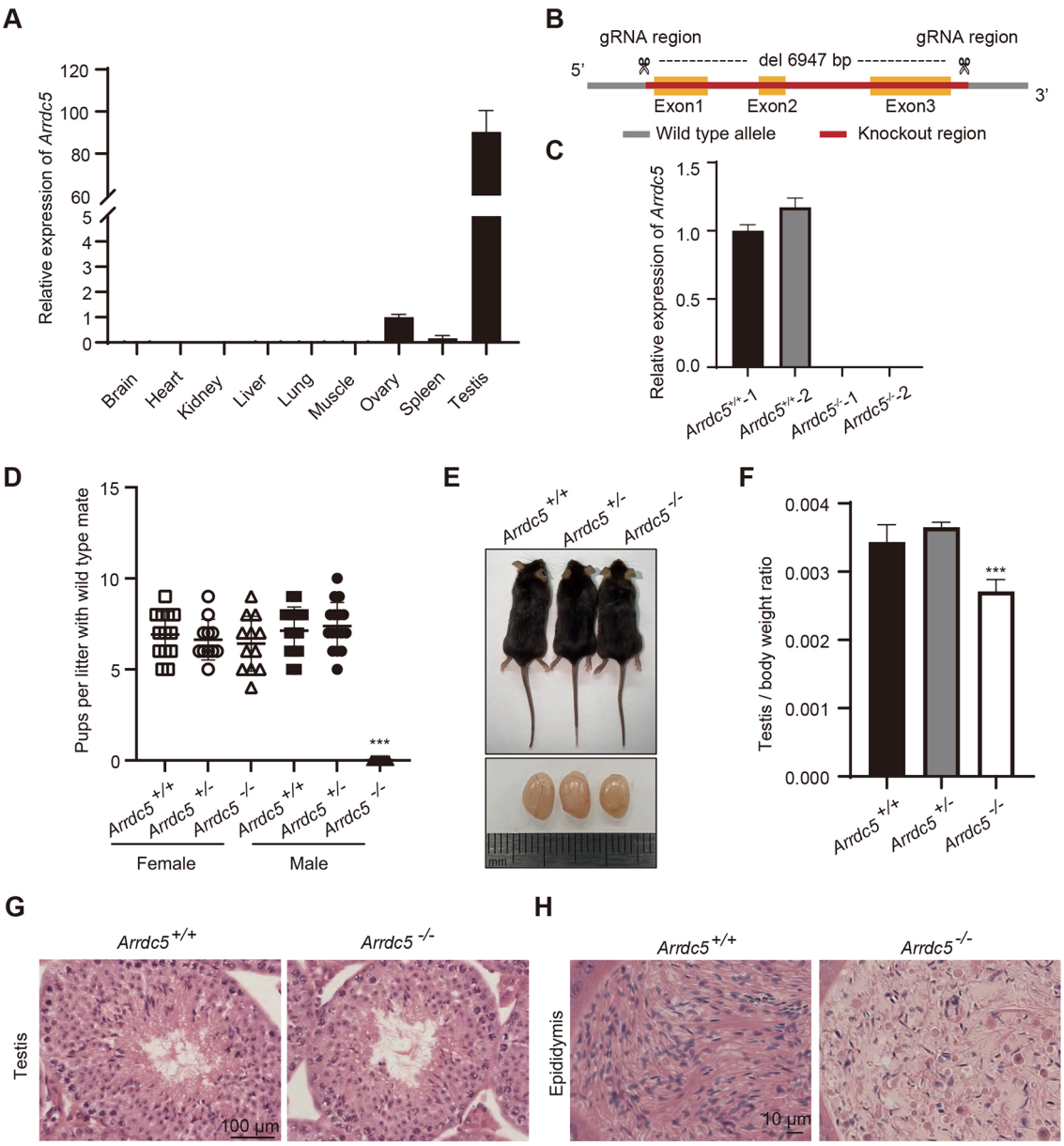

Fig. 1. *Arrdc5* is a testis-specific gene and is essential for male fertility. (A) The relative expression of *Arrdc5* in different tissues in mice. (B) The knockout strategy of *Arrdc5* in mice. (C) The relative expression of *Arrdc5* in testis from $Arrdc5^{+/+}$ and $Arrdc5^{-/-}$ mice. (D) The number of pups per litter in $Arrdc5^{+/+}$, $Arrdc5^{+/-}$ and $Arrdc5^{-/-}$ females and males mated with wild-type mice. The data are mean±s.d. ***P<0.001 (unpaired Student's t-test). At least three mice were used for each assay. n=13, 11, 12, 15, 16 and 13 observed litter numbers for each genotype. (E) The size of the testes in $Arrdc5^{+/+}$, $Arrdc5^{+/-}$ and $Arrdc5^{-/-}$ mice. Scale is in millimeters. (F) The ratio of testis weight/body weight in $Arrdc5^{+/+}$, $Arrdc5^{+/-}$ and $Arrdc5^{-/-}$ mice. Data are mean±s.d. ***P<0.001, n=4, 4 and 5 represent the number of mice weighed for each genotype. (G) Hematoxylin Eosin Saffron staining of the testis and cauda epididymis in $Arrdc5^{+/+}$ and $Arrdc5^{-/-}$ mice. (H) Hematoxylin and Eosin staining of cauda epididymis in $Arrdc5^{+/+}$ and $Arrdc5^{-/-}$ mice.

(Fig. 1D). The testis size and the ratio of testis weight to body weight were significantly reduced in $Arrdc5^{-/-}$ males compared with $Arrdc5^{+/+}$ and $Arrdc5^{+/-}$ males (Fig. 1E,F). Histologically, Hematoxylin Eosin Saffron staining of testis sections showed approximately intact spermatogenesis progression stages in $Arrdc5^{-/-}$ male mice (Fig. 1G), whereas sperm in the epididymis in $Arrdc5^{-/-}$ male mice showed a disorganized arrangement and reduced numbers (Fig. 1H).

To explore the effect of ARRDC5 depletion on sperm, we isolated the sperm from the cauda epididymis. The $Arrdc5^{-/-}$ sperm showed slower speed compared with control sperm. We then analyzed sperm mobility and found defects in ARRDC5 led to significantly reduced sperm motility (P<0.001) and progress rate (P<0.001) (Fig. 2A) together with reduced average path velocity (P=0.006), straight line velocity (P=0.002) and curvilinear velocity (P<0.001) (Fig. 2B). We further evaluated the morphology of the sperm. $Arrdc5^{-/-}$ sperm under light microscopy showed a significantly (P<0.001) higher bent-head rate (0.93±0.018, mean±s.d.) than wild-type sperm (0.091±0.045) (Fig. 2C,D); this was subsequently confirmed by scanning electron microscopy (SEM) (Fig. 2E). A few other anomalies of morphology were also observed in $Arrdc5^{-/-}$ sperm, such as abnormal head morphology (0.358±0.02) and double-headed sperm (0.027±0.01) (Fig. 2C,F). To explore the stage at which sperm defects occurred, we examined the testis by transmission electron microscopy (TEM). At

Development (2023) 150, dev201959. doi:10.1242/dev.201959

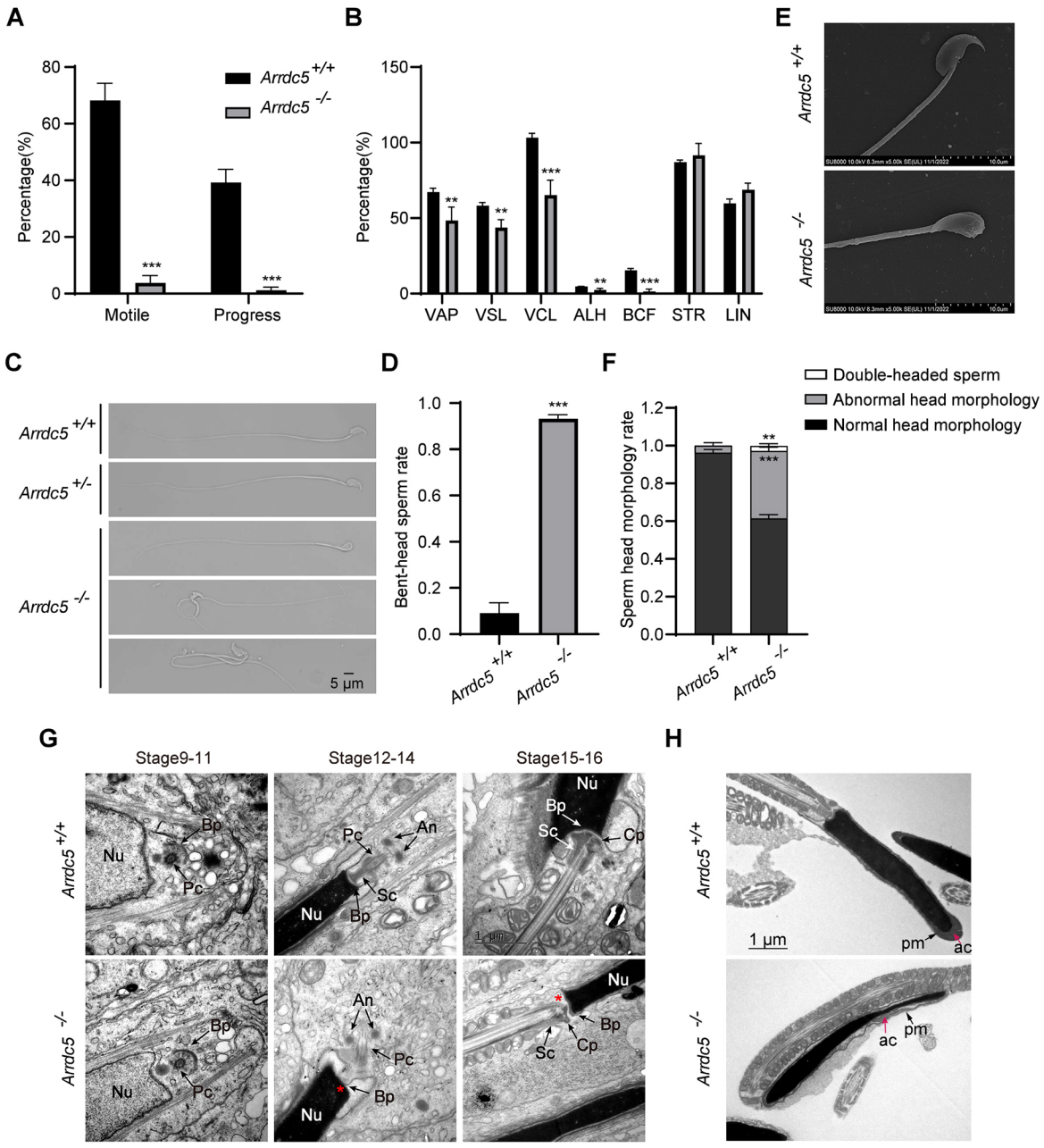

Fig. 2. ARRDC5 deficiency leads to reduced sperm motility, abnormal sperm morphology and spermatogenesis defects. (A) Comparison of overall motility and progressive motility in *Arrdc5*$^{+/+}$ and *Arrdc5*$^{-/-}$ mice. Data are mean±s.d. ***P<0.001, n=3 mice. (B) Comparison of the average path velocity (VAP), straight-line velocity (VSL), curvilinear velocity (VCL), amplitude of lateral head displacement (ALH), beat-cross frequency (BCF), straightness (STR) and linearity (LIN) in *Arrdc5*$^{+/+}$ and *Arrdc5*$^{-/-}$ mice. The data are mean±s.d. ***P<0.001, **P<0.01, *P<0.05 (multiple unpaired t-test), n=3 mice. (C) Images of *Arrdc5*$^{+/+}$, *Arrdc5*$^{+/-}$ and *Arrdc5*$^{-/-}$ sperm under light microscopy. Scale bar: 5 µm. (D) The bent-head rate in *Arrdc5*$^{+/+}$ and *Arrdc5*$^{-/-}$ sperm. The data are mean±s.d. ***P<0.001, n>200 sperm. (E) Scanning electron microscopy images of sperm morphology from *Arrdc5*$^{+/+}$ and *Arrdc5*$^{-/-}$ mice. Scale is in 10 µm increments. (F) The sperm head morphology rate in *Arrdc5*$^{+/+}$ and *Arrdc5*$^{-/-}$ sperm. Data are mean±s.d. **P<0.01, ***P<0.001, n>100 sperm. (G) Transmission electron microscopy (TEM) analysis of the stepwise development of the sperm-coupling apparatus in *Arrdc5*$^{+/+}$ and *Arrdc5*$^{-/-}$ testes. Nu, nucleus; Bp, basal plate; Cp, capitulum; Sc, segmented column; Pc, proximal centriole; An, annulus. (H) TEM analysis of mature sperm in the *Arrdc5*$^{+/+}$ and *Arrdc5*$^{-/-}$ cauda epididymis. ac, acrosome; pm, plasma membrane. Scale bar in H: 1 µm for G and H.

stage 12-14 of spermatogenesis, there was full and tight attachment between the head-tail coupling apparatus (HTCA) and the nuclear envelope in wild-type spermatids, whereas spermatids with ARRDC5 deficiency showed an incomplete and loose attachment that led to an offset angle between the head and tail (Fig. 2G). Meanwhile, we assessed manchettes during spermatogenesis, and the manchettes of *Arrdc5*$^{-/-}$ spermatids showed inaccurate and disheveled localization compare with wild-type spermatids (Fig. S1). This also partly indicated the role of ARRDC5 in intracellular transport. Correspondingly, mature sperm from the *Arrdc5*$^{-/-}$ cauda epididymis were affected and showed a bent head and other abnormalities in the SEM imaging (Fig. 2H). These results illustrate the importance of ARRDC5 for spermatogenesis, sperm morphology and sperm mobility.

Development (2023) 150, dev201959. doi:10.1242/dev.201959

Arrdc5$^{-/-}$ male mice experienced capacitation defects and IVF failure

We performed *in vitro* fertilization (IVF) to explore the reason for male mouse infertility and, as we expected, almost no two-pronuclear (2PN) zygotes were formed with *Arrdc5*$^{-/-}$ sperm (Fig. 3A,B). Immunofluorescence staining confirmed that most sperm were unable to penetrate into the zona pellucida (ZP) (Fig. 3C). We then measured the presence of protein tyrosine phosphorylation in sperm after incubation in human tubal fluid medium (HTF) to determine the ability for sperm capacitation. *Arrdc5*$^{-/-}$ sperm failed to capacitate, as indicated by reduced levels of protein tyrosine phosphorylation (Fig. 3D,E). These results indicated that ARRDC5 deletion impaired the sperm capacitation, which prevented the sperm from crossing the ZP, thus resulting in fertilization failure.

ARRDC5 is involved in spermatogenesis by affecting NDC1 and SUN5

To explore the molecular mechanism behind the role of ARRDC5 in spermatogenesis, we performed whole-protein mass spectrometry of adult wild-type and *Arrdc5*$^{-/-}$ testes to search for differentially expressed proteins. A total of 8193 proteins were scored, and the genes that encoded the top 300 downregulated proteins in *Arrdc5*$^{-/-}$ mice were selected for Gene Ontology (GO) term enrichment analysis (Fig. 4A,B, Fig. S2A,B). The GO analysis indicated that these proteins were highly enriched in the categories of protein transport and spermatogenesis (Fig. 4B).

Because *Arrdc5*$^{-/-}$ sperm showed bent heads and reduced motility, and based on the results of previous studies and reported mouse models, we focused on NDC1 and SUN5. NDC1 transmembrane nucleoporin (NDC1) has been shown to be

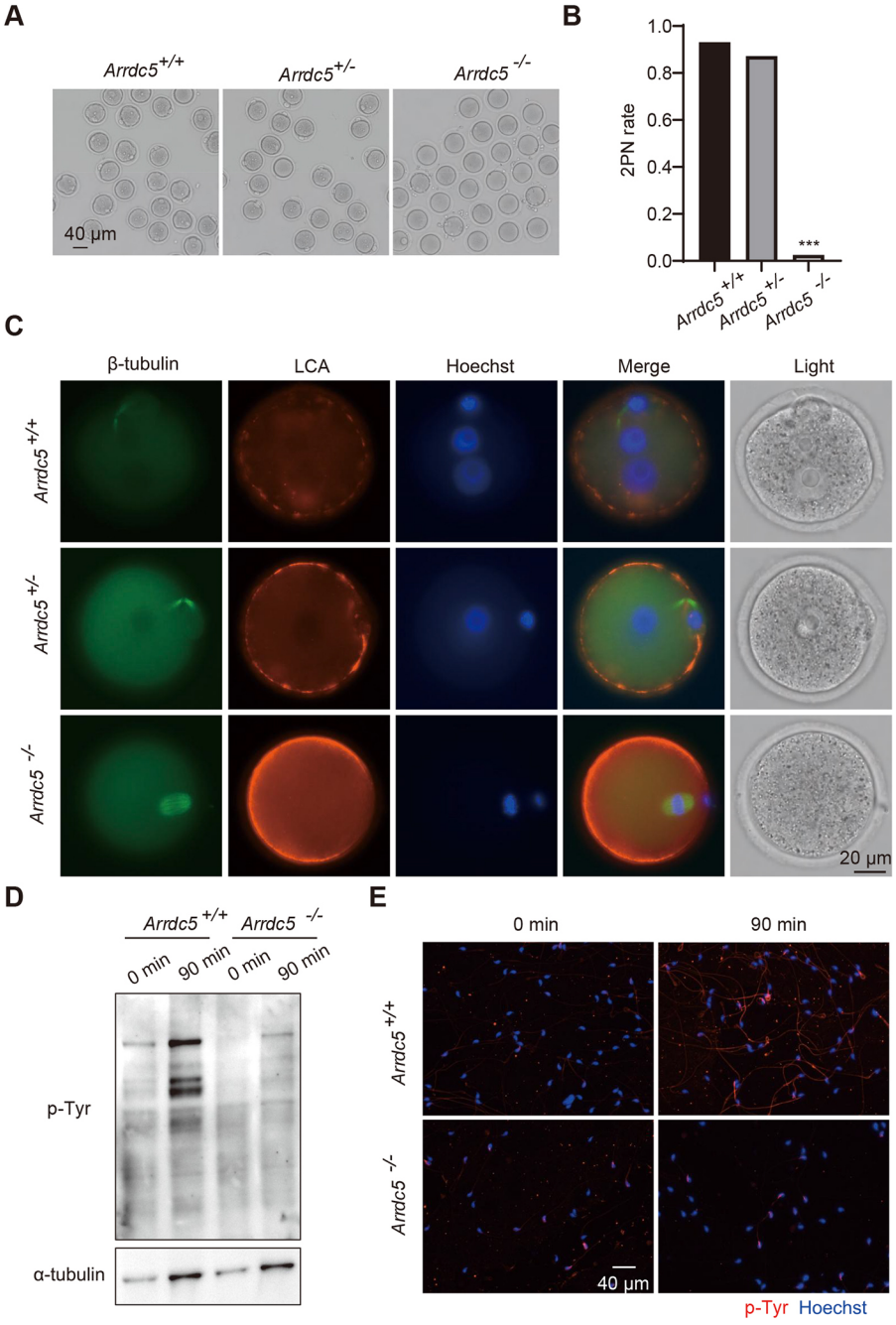

Fig. 3. Sperm with ARRDC5 deficiency lead to IVF failure and capacitation failure. (A) Representative 2PN zygotes resulting from fertilization of normal oocytes with *Arrdc5*$^{+/+}$, *Arrdc5*$^{+/-}$ and *Arrdc5*$^{-/-}$ sperm. Scale bar: 40 µm. (B) The 2PN rate from fertilized normal oocytes with *Arrdc5*$^{+/+}$, *Arrdc5*$^{+/-}$ and *Arrdc5*$^{-/-}$ sperm. The 2PN rate is shown as the percentage of 2PN zygotes out of the total oocytes. ***P<0.001 (χ^2 test). (C) Immunofluorescence staining of oocytes fertilized with *Arrdc5*$^{+/+}$ and *Arrdc5*$^{+/-}$ sperm but unfertilized with *Arrdc5*$^{-/-}$ sperm. β-Tubulin (green) shows the spindle, Hoechst 33342 (blue) shows the DNA and LCA (red) shows the cortical granules. Scale bar: 20 µm. (D) Western blotting of protein tyrosine phosphorylation to evaluate *Arrdc5*$^{+/+}$ and *Arrdc5*$^{-/-}$ sperm capacitation at 0 min and after 90 min of incubation with HTF. p-Tyr, protein tyrosine phosphorylation. (E) Immunofluorescence staining of protein tyrosine phosphorylation (red) to evaluate *Arrdc5*$^{+/+}$ and *Arrdc5*$^{-/-}$ sperm capacitation at 0 min and at 90 min of incubation with HTF. Hoechst 33342 (blue) shows the DNA. p-Tyr, protein tyrosine phosphorylation. Scale bar: 40 µm.

Development (2023) 150, dev201959. doi:10.1242/dev.201959

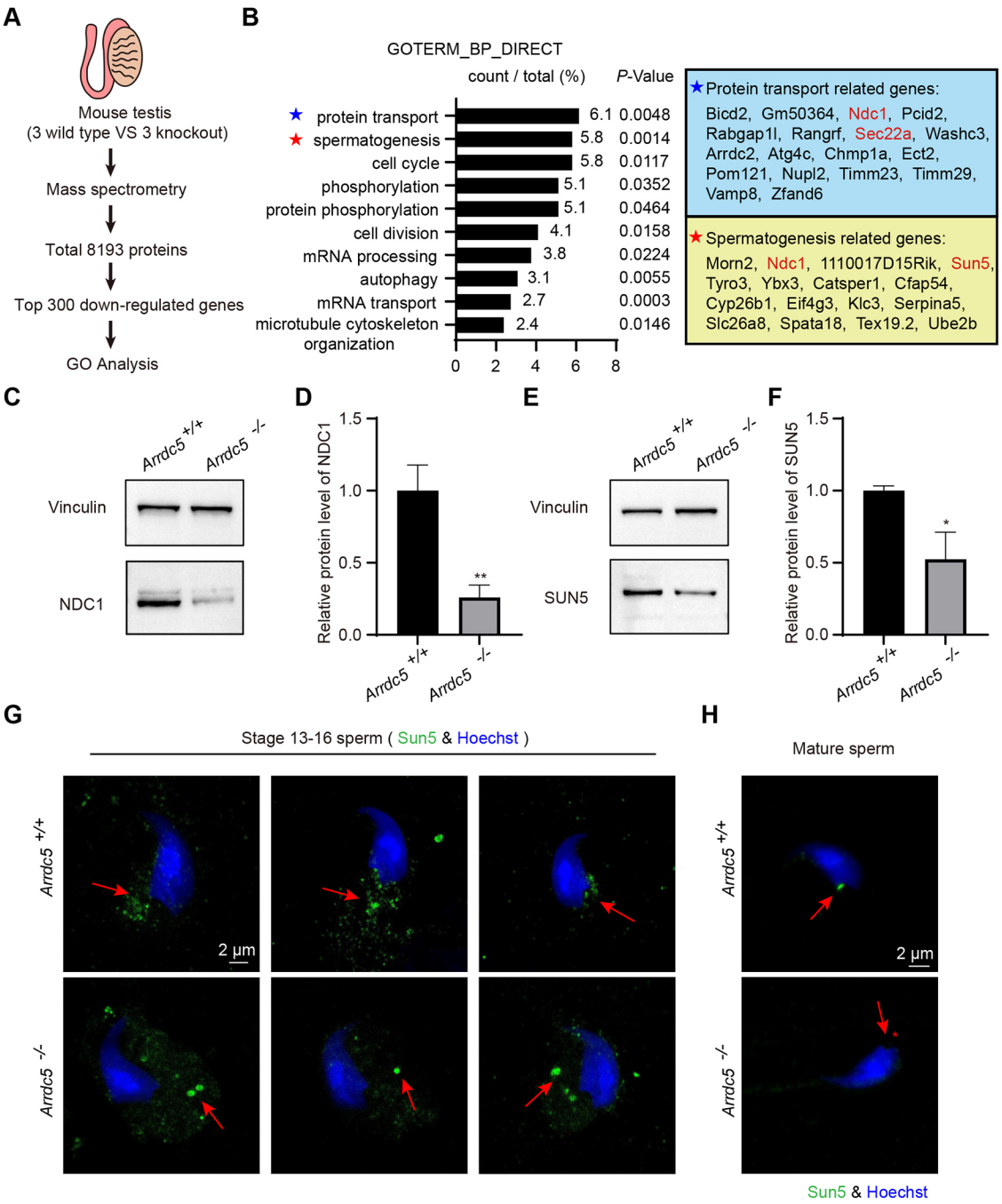

Fig. 4. Mass spectrometry and GO analysis suggest that ARRDC5 deficiency affects spermatogenesis due to reduced NDC1 and SUN5. (A) Flow chart of mouse testicular mass spectrometry and GO analysis. (B) Biological processes enriched in the GO analysis of the downregulated genes in *Arrdc5*$^{-/-}$ testis. (C,D) Western blotting (C) and quantification (D) of NDC1 in testis from *Arrdc5*$^{+/+}$ and *Arrdc5*$^{-/-}$ mice. **P<0.01 (unpaired t-test), n=3 for both *Arrdc5*$^{+/+}$ and *Arrdc5*$^{-/-}$. (E,F) Western blotting (E) and quantification (F) of SUN5 in testis from *Arrdc5*$^{+/+}$ and *Arrdc5*$^{-/-}$ mice. *P<0.05 (unpaired t-test), n=3 for both *Arrdc5*$^{+/+}$ and *Arrdc5*$^{-/-}$. (G) Immunofluorescence staining of SUN5 (green) for stage 13-16 sperm during spermatogenesis in *Arrdc5*$^{+/+}$ and *Arrdc5*$^{-/-}$ testes. Hoechst 33342 (blue) shows the DNA. Scale bar: 2 µm. Arrows indicate the different locations of SUN5 in *Arrdc5*$^{+/+}$ and *Arrdc5*$^{-/-}$ sperm. (H) Immunofluorescence staining of SUN5 (green) for mature sperm in the *Arrdc5*$^{+/+}$ and *Arrdc5*$^{-/-}$ cauda epididymis. Hoechst 33342 (blue) shows the DNA. Scale bar: 2 µm. The arrows indicate the location of SUN5; the asterisk indicates the absence of SUN5.

primarily expressed in the sperm neck between the sperm head and tail (Yeh et al., 2015). NDC1 is a regulator of SEPT12 function, and SEPT12-NDC1 complexes are involved in sperm head and tail formation during mammalian spermiogenesis (Lai et al., 2016). Western blotting showed about a 75% reduction (P=0.0029) of NDC1 protein levels in *Arrdc5*$^{-/-}$ testes (0.259±0.086, mean±s.d.) compared with *Arrdc5*$^{+/+}$ testes (1.000±0.178) (Fig. 4C,D), whereas there was no significant difference in mRNA level (Fig. S3A). Sad1 and UNC84 domain-containing 5 (SUN5) has been reported to play an essential role in anchoring the sperm head to the tail, and *Sun5*-null mice show a globozoospermatozoa-like acephalic spermatozoa (Shang et al., 2017; Zhang et al., 2021b). Western blotting showed about a 50% reduction (P=0.013) of SUN5 protein levels in *Arrdc5*$^{-/-}$ testes (0.524±0.188) compared

Development (2023) 150, dev201959. doi:10.1242/dev.201959

with *Arrdc5*$^{+/+}$ testes (1.000±0.033) (Fig. 4E,F), whereas there was no significant difference in mRNA level (Fig. S3B). Because SUN5 migrates to the coupling apparatus of the sperm during sperm head elongation and differentiation (Shang et al., 2017), we performed immunofluorescence staining in testis smears, and we found that ARRDC5 deficiency led to incorrect localization of SUN5 at stage 13-16 during spermatogenesis (Fig. 4G). Finally, mature sperm from the *Arrdc5*$^{-/-}$ cauda epididymis showed a bent head and no detectable SUN5 (Fig. 4H). Previous work has shown that NDC1 is involved in sperm head and tail formation during mammalian spermiogenesis and that SUN5 deletion causes similar defects in sperm head and tail anchoring as *Arrdc5* knockout mice sperm (Lai et al., 2016; Shang et al., 2017; Yeh et al., 2015; Zhang et al., 2021b). Taken together, we speculated that ARRDC5 might affect spermatogenesis by influencing NDC1 and SUN5.

ARRDC5 is a membrane protein involved in SEC22A-mediated NDC1 and SUN5 transport

Because ARRDC5 deletion caused a sharp decrease in the expression of NDC1 and SUN5 (Fig. 4C,E), we asked how ARRDC5 affects NDC1 and SUN5 during spermatogenesis. Previous studies (Zbieralski and Wawrzycka, 2022) have shown that ARRDC5 shares the overall arrestin-like domains with other α-arrestins (Fig. 5A), and immunofluorescence staining for overexpressed ARRDC5 in HeLa cells indicated that ARRDC5 is a membrane-bound protein. Furthermore, ARRDC3, another member of the α-arrestins, has been reported to be a membrane protein and to play a role in regulating the trafficking of G protein-coupled receptors (Tian et al., 2016; Zbieralski and Wawrzycka, 2022). These findings, combined with the GO analysis presented here suggest that ARRDC5 might have a similar function to ARRDC3 in protein transport. Therefore, we co-expressed ARRDC5 with other ARRDCs in HeLa cells and performed immunofluorescence staining. The results showed that ARRDC5 mainly localized on the cell membrane and co-localized with ARRDC3 and ARRDC4 (Fig. 5B), which supported our hypothesis that ARRCD5 might play a similar function as ARRDC3 and ARRDC4. Based on these results, we asked if ARRDC5 is directly involved in transporting NDC1 and/or SUN5. Thus, we co-expressed ARRDC5 with NDC1 and SUN5 in HeLa cells and performed immunofluorescence staining. However, ARRDC5 did not co-localize with either NDC1 or SUN5 (Fig. S4A, B), thus suggesting that ARRDC5 does not function by directly interacting with NDC1 and SUN5.

To determine how ARRDC5 affects NDC1 and SUN5, we further analyzed the candidate proteins enriched in the protein transport pathway (Fig. 4B). We found that the SEC22A protein was nearly undetectable in *Arrdc5*$^{-/-}$ testes according to our mass spectrometry results, but there was no significant difference in the mRNA level (Fig. S2C). SEC22 homolog A, a vesicle trafficking protein (SEC22), belongs to the SEC22 family of vesicle trafficking proteins, one of which (SEC22) has been reported to play diverse roles in vesicle trafficking, membrane fusion and autophagy (Adnan et al., 2019). Because SEC22A might play an intermediate role in protein transport, we hypothesized that ARRDC5 might participate in protein transport by affecting SEC22A. To test this hypothesis, we originally tried to validate the possible role of ARRDC5 in regulating SEC22A-mediated transportation in testis; however, owing to lack of a commercially available SEC22A antibody, we co-expressed SEC22A with ARRDC5, NDC1 and SUN5 in HeLa cells and performed immunofluorescence staining to validate the relationship between ARRDC5 and SEC22A. We found that SEC22A was partly co-localized with ARRDC5 and co-localized with NDC1 and SUN5 (Fig. 5C). Co-immunoprecipitation (co-IP) in HeLa cells also showed that SEC22A directly interacted with ARRDC5, NDC1 and SUN5 (Fig. 5D-F). Because SEC22A is a vesicle trafficking protein and is able to shuttle through cells, it is likely that SEC22A acts as a bridge to establish the link between ARRDC5 and NDC1 and SUN5.

ICSI can rescue fertilization failure

Despite *Arrdc5*$^{-/-}$ sperm showing bent heads and reduced motility, the structure of the entire head was relatively intact. We therefore performed ICSI to see whether it could rescue the fertilization failure of *Arrdc5*$^{-/-}$ sperm and found that *Arrdc5*$^{-/-}$ sperm could accomplish fertilization with wild-type oocytes and that the resulting embryos could ultimately develop into blastocysts (Fig. 6). The result suggested that ICSI might be a treatment strategy for male infertility due to ARRDC5 deficiency.

DISCUSSION

In this study, we revealed the important role of ARRDC5 in spermatogenesis by affecting the attachment of the HTCA to the nuclear envelope. Deficiency in ARRDC5 led to abnormal sperm morphology and failed capacitation, and thus a failure of fertilization. Our mechanistic studies revealed a possible pathway through which ARRDC5 affects SEC22A in a direct or indirect way, which carries NDC1, SUN5 and other HTCA-related proteins to the correct location and initiates the attachment of the sperm head and tail during spermatogenesis (Fig. 7). ARRDC5 deficiency likely disrupts this protein transport process, and the ectopic localization of NDC1, SUN5 and other HTCA-related proteins without SEC22A transport might be disrupted.

As we prepared this article, Giassetti et al. reported that ARRDC5 was required for normal sperm morphogenesis and male fertility (Giassetti et al., 2023). Both studies observed the abnormal morphology and reduced motility in *Arrdc5*$^{-/-}$ sperm with capacitation and fertilization failure. The study of Giassetti et al. demonstrated a conserved role in mammalian by analyzing expression of ARRDC5 was in multispecies testicular cells. Although our study carried out a deeper exploration and found the possible molecular mechanism by which ARRDC5 functions during spermatogenesis, by combining Giassetti et al.'s research with ours, we believe there will be a more complete explanation of the biological functions of ARRDC5 in mammals.

During spermiogenesis the HTCA mediates the integration of the sperm head and tail to ensure subsequent high-speed motility, and HTCA defects lead to the development of abnormal sperm (Wu et al., 2020). Several proteins related to the HTCA have been reported. SPATA6 is required for normal assembly of the sperm connecting piece and for the tight head-tail conjunction, and the absence of SPATA6 in mice impairs the development of the connecting piece (Yuan et al., 2015). PMFBP1 is essential for the attachment of the coupling apparatus to the sperm head, and humans with *PMFBP1* mutations and *Pmfbp1*-deficient mice have both been shown to suffer from acephalic spermatozoa syndrome (Zhu et al., 2018). A recent study showed that centlein (CNTLN) acts as a linker between SUN5 and PMFBP1 to maintain the integrity of the HTCA (Zhang et al., 2021a), and in our *Arrd5*$^{-/-}$ mouse testis, SUN5 had reduced protein levels and an incorrect localization; thus, we suspected that the protein would be degraded. However, the phenotype of *Arrdc5* knockout sperm during spermatogenesis is not as severe as that of *Sun5*-null mice, and we suspect that this might be due to the dose of protein levels. Low doses of SUN5 may also provide weak support for HTCA assembly. Although the HTCA can be assembled according to our

Development (2023) 150, dev201959. doi:10.1242/dev.201959

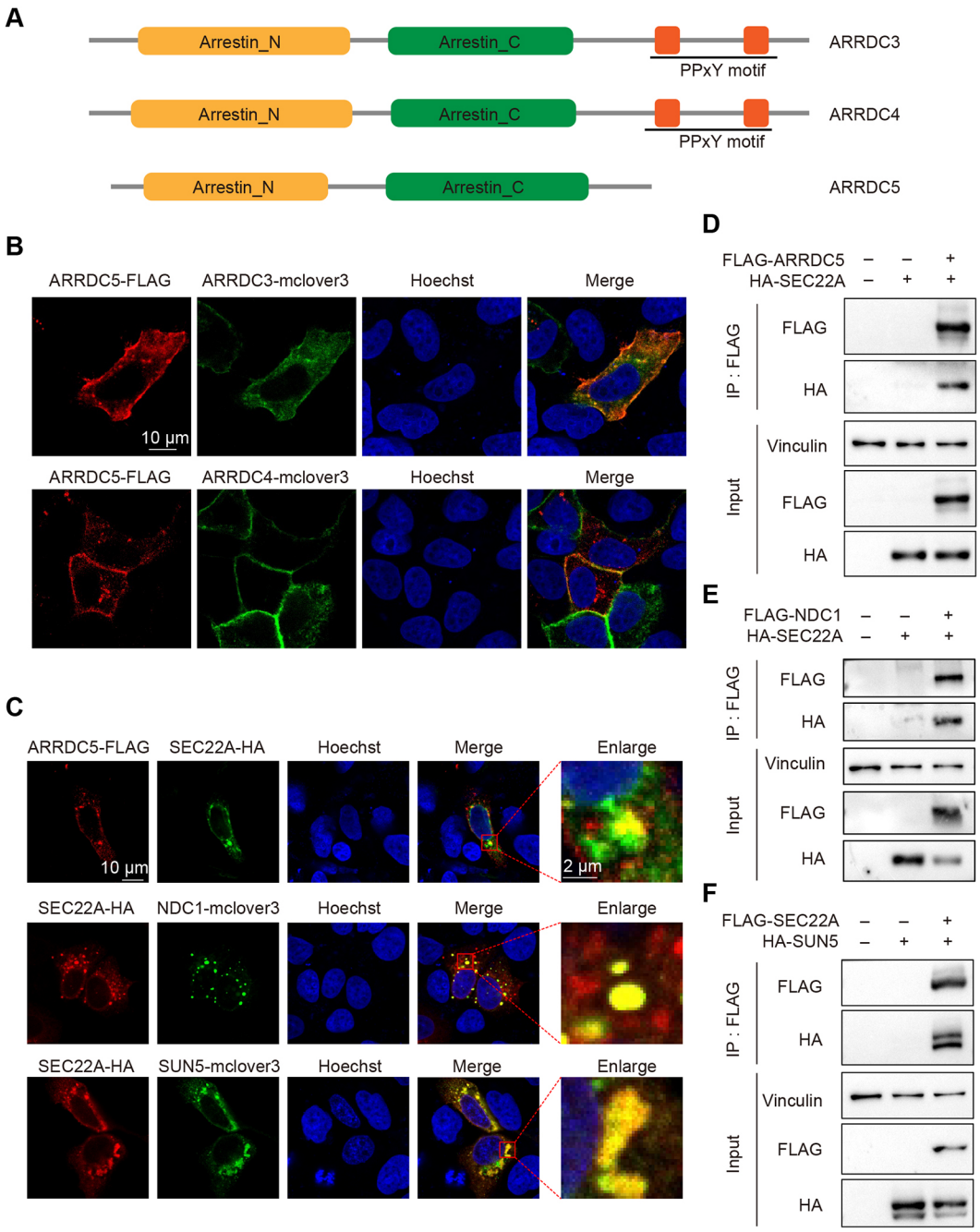

Fig. 5. ARRDC5 affects SEC22A-mediated protein transport, which in turn affects spermatogenesis. (A) Schematic representation of the domain structure of ARRDC3, ARRDC4 and ARRDC5 in mice. (B) Immunofluorescence staining of ARRDC5 with FLAG tag (red), ARRDC3 with mclover3 tag (green, top row) and ARRDC4 with mclover3 tag (green, bottom) in HeLa cells. Hoechst 33342 (blue) was used to visualize the DNA. Scale bar: 10 µm. (C) Immunofluorescent staining of ARRDC5 with a FLAG tag, SEC22A with a HA tag, NDC1 with a mclover3 tag and SUN5 with a mclover3 tag in HeLa cells. Hoechst 33342 (blue) was used to visualize the DNA. Scale bars: 10 µm (left) and 2 µm (right). (D) ARRDC5 interacted with SEC22A in cultured HeLa cells. (E) SEC22A interacted with NDC1 in cultured HeLa cells. (F) SEC22A interacted with SUN5 in cultured HeLa cells.

TEM results, it cannot fully attach to the nuclear envelope, which may be the reason for the sperm head hanging with a loose anchoring, which results in the bent-head phenotype.

The mass spectrometry and GO analysis suggested that many other proteins associated with spermatogenesis and sperm function are also affected by ARRDC5 deficiency. For example, *Serpina5* knockout mice are infertile due to abnormal spermatogenesis resulting from destruction of the Sertoli cell barrier (Uhrin et al., 2000), and blocking the SERPINA5 protein reduces the success rate of IVF and reduces the number of sperm that combine with the ZP of oocytes (Cao et al., 2022). SERPINA5 also showed a sharp reduction in expression in the *Arrdc5*$^{-/-}$ testis in this study, which might be another possible reason for the fertilization failure with *Arrdc5*$^{-/-}$ sperm. SPATA18 has also been reported to be associated with spermatogenesis (Bornstein et al., 2011), and SPATA18 protein expression was also reduced in the *Arrdc5*$^{-/-}$ testis. POM121 is a transmembrane nucleoporin that, together with nucleoporin 210 (NUP210) and NDC1, forms a ring

Development (2023) 150, dev201959. doi:10.1242/dev.201959

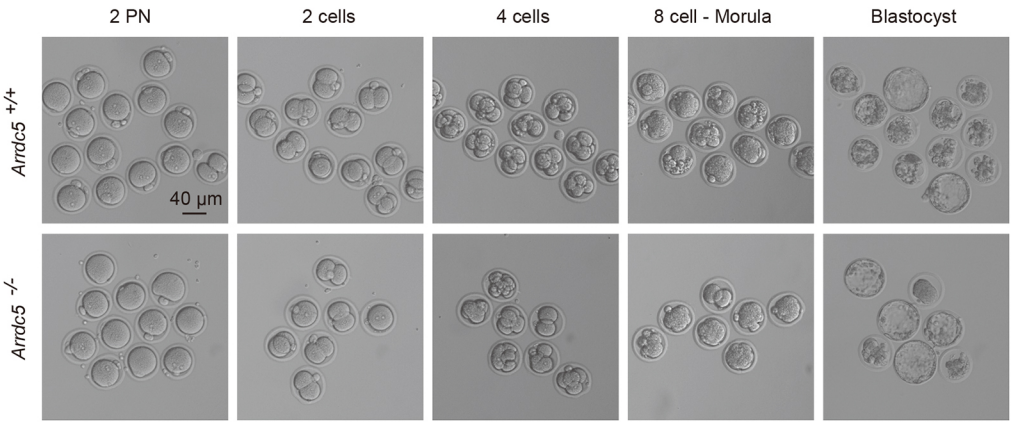

Fig. 6. ICSI can rescue *Arrdc5*$^{-/-}$ fertilization defects. Light micrographs of early embryonic development after ICSI using *Arrdc5*$^{+/+}$ and *Arrdc5*$^{-/-}$ sperm heads. Scale bar: 40 µm.

of transmembrane nucleoproteins and helps nuclear pore complexes anchor to the nuclear envelope (Strambio-De-Castillia et al., 2010). Both POM121 and NDC1 were reduced in *Arrdc5*$^{-/-}$ testis, so it might be the combined loss of the two proteins that results in abnormal formation of sperm head-tail junctions during spermatogenesis. On the other hand, TCP11 has been reported to be important for sperm progressive motility and sperm capacitation through the cyclic AMP/protein kinase A pathway (Castaneda et al., 2020; Fraser et al., 1997). We found that TCP11 was also reduced in the *Arrdc5*$^{-/-}$ testis, which we suspected might affect the capacitation of *Arrdc5*$^{-/-}$ sperm. All of these proteins can be further studied in the future to gain a more comprehensive understanding of spermatogenesis.

The high conservation of ARRDC5 in mammalian species and our studies on ARRDC5 in mouse models suggest an essential role for ARRDC5 in spermatogenesis in mice. In addition, we show that ARRDC5 might be involved in the anchoring of the sperm head to the tail during spermatogenesis by affecting SEC22A-mediated SUN5 and NDC1 transport and localization. These findings suggest that ARRDC5 might be a new genetic marker for pathogenic variant-targeted sequencing in individuals with similar phenotypes. Finally, we found that ICSI enabled successful rescue of fertility, thus suggesting a therapeutic strategy with which to overcome male infertility caused by ARRDC5 deficiency.

MATERIALS AND METHODS

Animals

All of our animal experiments were approved by the Ethics Committee of the Medical College of Fudan University and followed all animal testing guidelines and regulations. The mice were euthanized by cervical dislocation according to *The AVMA Guidelines for the Euthanasia of Animals: 2020 Edition*. The approval number associated with the use of mice is 2021JSIBS-007 of Fudan University.

Plasmids

We fused the coding sequences from mouse tissue cDNA template with FLAG, mclover3 and HA, and inserted them into the pXF4H, pCR3.1 or pCMV6 plasmids to obtain pXF4H-*Arrdc5*-FLAG, pXF4H-*sec22a*-FLAG, pXF4H-*ndc1*-HA, pXF4H-*sun5*-HA, pCR3.1-*Arrdc5*-FLAG, pCR3.1-*Arrdc3*-mclover3, pCR3.1-*Arrdc4*-mclover3, pCR3.1-*Sun5*-mclover3, pCR3.1-*Ndc1*-mclover3 and pCMV6-*Sec22a*-HA.

Antibodies

Primary antibodies were rabbit anti-SUN5 (17495-1-AP, Proteintech), anti-NDC1 (A17727, Abclonal), anti-vinculin (1390T, CST, Danvers), anti-HA (3724T, CST), anti-FLAG (F7425, Sigma-Aldrich), anti-α-Tubulin (T6199, Sigma-Aldrich), mouse anti-FLAG (GNI4110-FG, GNI) and anti-phosphotyrosine (ab10321, Abcam).

Cell culture and transfections

The HeLa cell line was obtained from the Cell Bank of the Shanghai Institute for Biological Sciences, the Chinese Academy of Sciences (Shanghai, China).

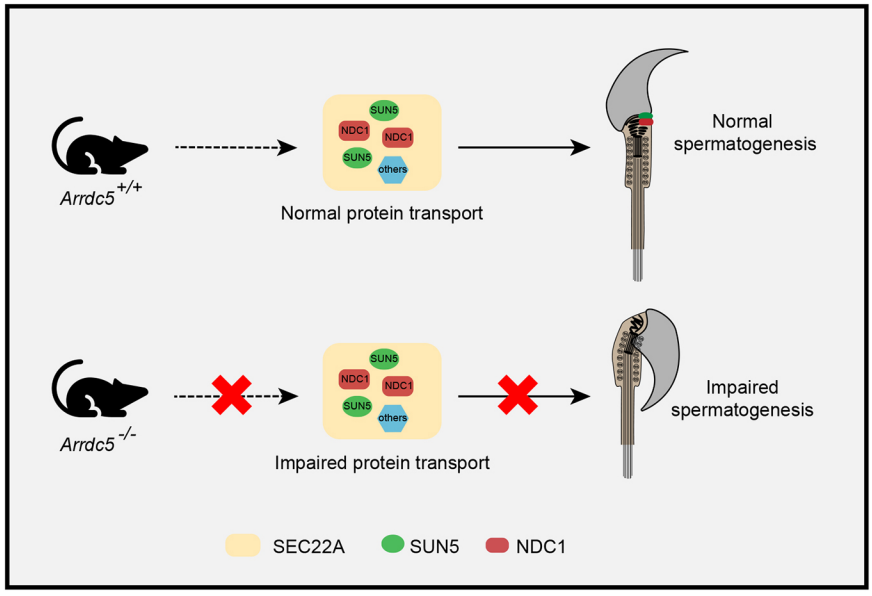

Fig. 7. Schematic diagram of the effects of ARRDC5 on spermatogenesis. In the mouse testis, ARRDC5 affects spermatogenesis in either a direct (top) or indirect (bottom) way. ARRDC5 produces SEC22A-mediated localization of NDC1, SUN5 and other HTCA-related proteins, which indirectly leads to proper attachment of the sperm head and tail during spermatogenesis. ARRDC5 deficiency directly disrupts this protein transport process and sperm eventually show abnormal morphology.

Development (2023) 150, dev201959. doi:10.1242/dev.201959

HeLa cells were cultured in high-glucose Dulbecco's modified Eagle's medium (DMEM, Gibco) supplemented with 10% fetal bovine serum (F2442, Sigma-Aldrich) and 1% penicillin and streptomycin (Gibco) at 37°C with 5% CO_2. Transfection of plasmids was performed with PolyJet (SL100688, SignaGen Laboratories) according to the manufacturer's instructions.

Generation of *Arrdc5* knockout mice

The *Arrdc5*$^{-/-}$ mice were generated by CRISPR/Cas-mediated genome engineering in the C57BL/6J mouse model (constructed by Cyagen Biosciences). The Cas9 and gRNA (Table S1) were co-injected into fertilized mouse eggs to generate targeted knockout offspring. F0 founder animals were genotyped by PCR followed by sequence analysis and were bred until homozygous knockout offspring were obtained.

Sperm motility analysis

Sperm for motility was referred to Martinez (Martinez, 2022). Sperm from the mouse cauda epididymis were backflushed and incubated in M2 medium for 15 min at 37°C to gain motility. The sperm were subsequently homogenized and transferred to a Leja slide, and their concentration and motility characteristics were assessed using a computer-assisted sperm analysis system (Hamilton Thorne IVOS II).

Scanning electron microscopy and transmission electron microscopy

Sample preparation was performed according to a previously described method (Zhang et al., 2023). For scanning electron microscopy (SEM), washed sperm of adult male mice were spread on a 2×3mm glass slide and air dried. The glass slides were then fixed with 2.5% (vol/vol) glutaraldehyde at 4°C overnight. Images were obtained on an SU801microscope (HITACHI SU8010, Japan) according to standard SEM procedures.

For transmission electron microscopy (TEM), the dissected testes and washed sperm of adult male mice were fixed with 2.5% (vol/vol) glutaraldehyde at 4°C overnight. Tissues were cut into small pieces of ∼1 mm^3 and immersed in 1% OsO_4 for 2 h at 4°C. The samples were dehydrated through graded ethanol and acetone, and finally embedded in resin for ultrathin sectioning with an ultramicrotome. The samples were then stained with uranyl acetate and lead citrate, and photographed using a Philips CM-120.

Real-time PCR (qRT-PCR)

Total RNA from mouse tissues were extracted using an RNeasy Mini Kit (Qiagen). After genomic DNA depletion, 1 µg RNA was used for reverse transcription using a PrimeScript RT reagent Kit with gDNA Eraser (RR047B, TaKaRa). The primer concentration was 50 pmol/ 20 µl. The reverse transcriptase was in the PrimeScript RT Enzyme Mix and the concentration was 200 U/µl. The cDNA sample was diluted 10-fold for qRT-PCR. qRT-PCR was performed using a Quant Studio 5 Real-Time PCR System (Applied Biosystems, Thermo Fisher Scientific), with TaKaRa TB Green Premix Ex Taq (Tli RNaseH Plus). The PCR reactions were performed as follows: hold stage, 50°C for 2 min and 95°C for 2 min; PCR stage, 40 cycles of 95°C for 10 s and 60°C for 30 s; melt curve stage, 95°C for 15 s, 60°C for 1 min and 95°C for 15 s. Design and Analysis Software v2.6.0 (Thermo Fisher Scientific) was used for qPCR analysis. Cq values<38 and Cq shift within 0.5 was valid. *Actb* and *Gapdh* were chosen as two housekeeping genes by the Minimum Information for Publication of Quantitative Real-Time PCR Experiments (MIQE) guidelines (Bustin et al., 2009). The relative expression level equaled $k\times2^{-\Delta\Delta Cq}$, where ΔCq=(Cq (*candidate gene*) – Cq (*housekeeping genes*)) – ((CqWT(*candidate gene*)−CqWT (*housekeeping genes*)) (Pfaffl, 2001). For comparison of related gene expression in wild-type and knockout testes, wild type was chosen as a reference gene and normalized as 1 for relative expression level. Four technical replicates were performed for each sample assay. qPCR specificity has been validated (Fig. S5A,B and Table S2).

Fertility test

At 6-8 weeks of age, C57BL/6J wild-type female mice were mated with 10- to 12-week-old wild-type and knockout male mice for 4 months (two females per male). The vaginal plugs of the female mice were checked to confirm their mating. The number of litters and pups per litter were calculated, and Student's *t*-test was performed to compare averages in different experimental groups. $P<0.05$ was considered to be significant.

IVF

At 7-8 weeks of age CD-1 (ICR) female mice were superovulated by injecting pregnant mare serum gonadotropin (Ningbo Second Hormone Factory, Zhejiang, China) followed by human chorionic gonadotropin (Ningbo Second Hormone Factory, Zhejiang, China) 46-48 h later. After 12 h, sperm were collected from the cauda epididymis of male mice and capacitated in a drop of HTF at 37°C with 5% CO_2 for 1 h. Cumulus-oocyte complexes from superovulated female mice were then fertilized with capacitated sperm in a drop of HTF at 37°C with 5% CO_2 for 6 h, after which the 2PN zygotes were selected and transferred into KSOM medium (M1430, EasyCheck) at 37°C with 5% CO_2 for blastocyst culture.

ICSI

At 7-8 weeks of age B6D2F1 (C57BL/6×DBA2) female mice were superovulated as described above. After 13 h, sperm were collected from the cauda epididymis of male mice and capacitated in HTF using the swim up method at 37°C with 5% CO_2 for 1 h. Oocytes were collected from superovulated female mice and then freed from the cumulus by treatment with hyaluronidase (H4272, Sigma-Aldrich). Sperm preparation before injection was performed according to a previously described method (Kimura and Yanagimachi, 1995). The sperm were decapitated by ultrasonication (Skymen JP020S), and then single sperm heads were injected into the oocytes using a micromanipulator with a Piezo apparatus (Eppendorf). Injected oocytes were transferred into KSOM medium at 37°C with 5% CO_2 for subsequent development.

Mass spectrometry of testis

Testes from three pairs of wild-type and knockout mice were homogenized in RIPA lysis buffer (WB0101, Shanghai Wei AO Biological Technology) with 1% protease inhibitor cocktail (B14001, Bimake). The protein lysate was analyzed by mass spectrometry-based label-free quantitative proteomics commissioned by the Key Laboratory of Glycoconjugates Research Ministry of Public Health and Institutes of Biomedical Sciences of Fudan University. The database search was performed using mouse protein sequences obtained from UniProt allowing up to two missed cleavages. Fold change and false discovery rate values were calculated to analyze the expression of different proteins. Statistical analysis was performed using the Limma Bioconductor package to define the probability of variation (*P*-value) of each protein between two groups. Proteins with $P<0.05$ were considered significantly different (Tardif et al., 2022; van Ooijen et al., 2018). GO term enrichment analysis was performed using DAVID Bioinformatics Resources (https://david.ncifcrf.gov/), including biological processes (in the process, BP), molecular function (MF) and cell component (CC) enrichment. *P*-value cutoff=0.05 and the rest defaulted to original settings. The top 10 of BP, CC and MF were chosen for analysis.

Western blotting

The proteins from mouse testes were extracted using RIPA lysis buffer with 1% protease inhibitor cocktail, and the supernatants were collected after centrifugation at 12,000 **g** for 10 min. The protein concentration was quantified by the bicinchoninic acid method, and equal amounts of protein were separated by 10% SDS-PAGE gels and transferred onto nitrocellulose filter membranes. The membranes were blocked in 5% non-fat milk for 1 h and incubated with primary antibodies overnight at 4°C, and subsequent secondary antibody incubation was performed to detect the primary antibodies. The blots were finally captured using ECL western blotting substrate (180-5001, Tanon). The intensity and quantitation of western blotting results was measured by ImageJ/FIJI (NIH) (Schindelin et al., 2012) from three pairs of independent biological samples. Normal IgG antibodies and originals of western blotting are shown in Fig. S6A,B, Fig. S7 and Fig. S8.

Co-immunoprecipitation

Plasmids with FLAG-tag were co-transfected with the plasmids with HA-tag into HeLa cells. At 36 h after transfection, cell proteins were extracted

Development (2023) 150, dev201959. doi:10.1242/dev.201959

with NP-40 lysis buffer (50 mM Tris, 150 mM NaCl and 0.5% NP-40 at pH 7.5) containing 1% protease inhibitor cocktail (Bimake). Total protein was incubated with anti-FLAG beads (B23102, Bimake) at 4°C for 3 h. The beads were washed with lysis buffer three times and then boiled with SDS loading buffer for western blotting with anti-FLAG (1:3000 dilution) and anti-HA antibodies (1:3000 dilution).

Isolation of spermatogenic cells

Round spermatids and elongated spermatids from adult mouse testes were isolated according to a previous study (Bai et al., 2018). Briefly, the testicular tissues were stripped from the albuginea membrane and digested with collagenase IV (1 mg/ml, C4-BIOC, Sigma-Aldrich) for 10 min at 37°C. The dispersed testicular tissues were washed with DMEM and centrifuged at 500 **g**. The pellet was further digested with 0.25% Trypsin (Gibco) containing DNase I (1 mg/ml, M0303L, NEB) for 10 min at 37°C and centrifuged at 500 **g**. The pellet was then resuspended in DMEM and obtained a mixture of spermatogenic cells.

Immunofluorescence staining

Testicular spermatogenic cells were spread on glass slides and fixed in 4% PFA at room temperature for 15 min, rinsed in PBS three times, permeabilized in 0.3% Triton X-100 in PBS for 30 min and then blocked with blocking buffer (3% BSA in PBS) for 1 h at room temperature. The primary antibody was added and incubated at 4°C overnight, followed by incubation with secondary antibody (1:500 dilution) for 1 h at 37°C. Hoechst 33342 (1:500 dilution, 561908, BD Biosciences) was added for 15 min at room temperature to label the DNA. All images were captured on a laser scanning confocal microscope (LSM 880 with Airyscan, Zeiss).

For 2PN zygotes and unfertilized meiotic oocytes, the immunofluorescence staining was performed as described previously (Liu et al., 2022). Briefly, 2PN zygotes and unfertilized meiotic oocytes were fixed with 2% PFA, then permeabilized in 0.5% Triton X-100 and then blocked with blocking buffer (3% BSA, 0.1% Tween 20 and 0.01% Triton X-100 in PBS). Spindles were stained with an anti-β-tubulin antibody (1:500 dilution, F2043, Sigma-Aldrich). Cortical granules were stained with Lens Culinaris Agglutinin (DyLight 649 DL-1048-1) and Hoechst 33342 (1:500 dilution, MedChemExpress) was added to label the DNA. All images were captured on an EVOS M7000 Imaging System (Invitrogen). Normal IgG antibodies of immunofluorescence staining are shown in Fig. S6C,D.

Statistical analysis

All data are mean±s.d. Statistical analysis was performed using Prism GraphPad 9 software. The statistical significance was analyzed using a two-tailed Student's *t*-test or a χ^2 test, and $P<0.05$ was considered statistically significant. Quantitation of western blotting results was performed using ImageJ software, and all results shown are representative of at least three independent experiments.

Acknowledgements

We thank Yinghua Jiang for providing help with confocal imaging and the Public Technology Platform of Shanghai Medical College.

Competing interests

The authors declare no competing or financial interests.

Author contributions

Conceptualization: L.W., Q.S.; Methodology: R.L., R.Q., Y.Z., Y.L., F.X.; Formal analysis: Q.L., B.C., J.M.; Data curation: Q.L., B.C., J.M.; Writing - original draft: R.L.; Writing - review & editing: L.W., Z.Z., Q.S.; Project administration: R.L.

Funding

This work was supported by the National Key Research and Development Program of China for Young Scientists (2022YFC2702300), New Cornerstone Science Foundation through the XPLORER PRIZE, the National Natural Science Foundation of China (32130029 and 82201767) and a project of the Science and Technology Commission of Shanghai Municipality (21XD1420300 and 21YF1418300).

Data availability

All the data underlying this article are available in the article and in its online supplementary material.

Reference

Adnan, M., Islam, W., Zhang, J., Zheng, W. and Lu, G. D. (2019). Diverse role of SNARE protein Sec22 in vesicle trafficking, membrane fusion, and autophagy. *Cells* **8**, 337. doi:10.3390/cells8040337

Alvarez, C. E. (2008). On the origins of arrestin and rhodopsin. *BMC Evol. Biol.* **8**, 222. doi:10.1186/1471-2148-8-222

Bai, S., Fu, K., Yin, H., Cui, Y., Yue, Q., Li, W., Cheng, L., Tan, H., Liu, X., Guo, Y. et al. (2018). Sox30 initiates transcription of haploid genes during late meiosis and spermiogenesis in mouse testes. *Development* **145**, dev164855. doi:10.1242/dev.164855

Bornstein, C., Brosh, R., Molchadsky, A., Madar, S., Kogan-Sakin, I., Goldstein, I., Chakravarti, D., Flores, E. R., Goldfinger, N., Sarig, R. et al. (2011). SPATA18, a spermatogenesis-associated gene, is a novel transcriptional target of p53 and p63. *Mol. Cell. Biol.* **31**, 1679-1689. doi:10.1128/MCB.01072-10

Bustin, S. A., Benes, V., Garson, J. A., Hellemans, J., Huggett, J., Kubista, M., Mueller, R., Nolan, T., Pfaffl, M. W., Shipley, G. L. et al. (2009). The MIQE guidelines: minimum information for publication of quantitative real-time PCR experiments. *Clin. Chem.* **55**, 611-622. doi:10.1373/clinchem.2008.112797

Cao, S., Qian, Z., Wu, R., Sun, S., Jing, J., Zhang, G., Chen, W., Ge, Y., Ma, J., Wang, S. et al. (2022). SERPINA5 protein in cumulus-oocyte complexes increases the fertilisation ability of mouse sperm. *Reprod. Sci.* **29**, 2350-2362. doi:10.1007/s43032-022-00867-5

Castaneda, J. M., Miyata, H., Archambeault, D. R., Satouh, Y., Yu, Z., Ikawa, M. and Matzuk, M. M. (2020). Mouse t-complex protein 11 is important for progressive motility in sperm†. *Biol. Reprod.* **102**, 852-862. doi:10.1093/biolre/ioz226

Foot, N. J., Gonzalez, M. B., Gembus, K., Fonseka, P., Sandow, J. J., Nguyen, T. T., Tran, D., Webb, A. I., Mathivanan, S., Robker, R. L. et al. (2021). Arrdc4-dependent extracellular vesicle biogenesis is required for sperm maturation. *J. Extracell. Vesicles* **10**, e12113. doi:10.1002/jev2.12113

Fraser, L. R., Hosseini, R., Hanyalogou, A., Talmor, A. and Dudley, R. K. (1997). TCP-11, the product of a mouse t-complex gene, plays a role in stimulation of capacitation and inhibition of the spontaneous acrosome reaction. *Mol. Reprod. Dev.* **48**, 375-382. doi:10.1002/(SICI)1098-2795(199711)48:3<375::AID-MRD11>3.0.CO;2-V

Giassetti, M. I., Miao, D., Law, N. C., Oatley, M. J., Park, J., Robinson, L. D., Maddison, L. A., Bernhardt, M. L. and Oatley, J. M. (2023). ARRDC5 expression is conserved in mammalian testes and required for normal sperm morphogenesis. *Nat. Commun.* **14**, 2111. doi:10.1038/s41467-023-37735-y

Gurevich, V. V., Dion, S. B., Onorato, J. J., Ptasienski, J., Kim, C. M., Sterne-Marr, R., Hosey, M. M. and Benovic, J. L. (1995). Arrestin interactions with G protein-coupled receptors: direct binding studies of wild type and mutant arrestins with rhodopsin, β2-adrenergic, and m2 muscarinic cholinergic receptors (*). *J. Biol. Chem.* **270**, 720-731. doi:10.1074/jbc.270.2.720

Hao, S. L., Ni, F. D. and Yang, W. X. (2019). The dynamics and regulation of chromatin remodeling during spermiogenesis. *Gene* **706**, 201-210. doi:10.1016/j.gene.2019.05.027

Kimura, Y. and Yanagimachi, R. (1995). Intracytoplasmic sperm injection in the mouse. *Biol. Reprod.* **52**, 709-720. doi:10.1095/biolreprod52.4.709

Lai, T. H., Wu, Y. Y., Wang, Y. Y., Chen, M. F., Wang, P., Chen, T. M., Wu, Y. N., Chiang, H. S., Kuo, P. L. and Lin, Y. H. (2016). SEPT12-NDC1 complexes are required for mammalian spermiogenesis. *Int. J. Mol. Sci.* **17**, 1911. doi:10.3390/ijms17111911

Liu, R., Yan, Z., Fan, Y., Qu, R., Chen, B., Li, B., Wu, L., Wu, H., Mu, J., Zhao, L. et al. (2022). Bi-allelic variants in KCNU1 cause impaired acrosome reactions and male infertility. *Hum. Reprod.* **37**, 1394-1405. doi:10.1093/humrep/deac102

Martinez, G. (2022). First-line evaluation of sperm parameters in mice (Mus musculus). *Bio-protocol* **12**, e4529. doi:10.21769/BioProtoc.4529

Pfaffl, M. W. (2001). A new mathematical model for relative quantification in real-time RT-PCR. *Nucleic Acids Res.* **29**, e45. doi:10.1093/nar/29.9.e45

Schindelin, J., Arganda-Carreras, I., Frise, E., Kaynig, V., Longair, M., Pietzsch, T., Preibisch, S., Rueden, C., Saalfeld, S., Schmid, B. et al. (2012). Fiji: an open-source platform for biological-image analysis. *Nat. Methods* **9**, 676-682. doi:10.1038/nmeth.2019

Shang, Y., Zhu, F., Wang, L., Ouyang, Y. C., Dong, M. Z., Liu, C., Zhao, H., Cui, X., Ma, D., Zhang, Z. et al. (2017). Essential role for SUN5 in anchoring sperm head to the tail. *Elife* **6**, e28199. doi:10.7554/eLife.28199

Strambio-De-Castillia, C., Niepel, M. and Rout, M. P. (2010). The nuclear pore complex: bridging nuclear transport and gene regulation. *Nat. Rev. Mol. Cell Biol.* **11**, 490-501. doi:10.1038/nrm2928

Tanaka, H. and Baba, T. (2005). Gene expression in spermiogenesis. *Cell. Mol. Life Sci.* **62**, 344-354. doi:10.1007/s00018-004-4394-y

Tardif, G., Paré, F., Gotti, C., Roux-Dalvai, F., Droit, A., Zhai, G., Sun, G., Fahmi, H., Pelletier, J. P. and Martel-Pelletier, J. (2022). Mass spectrometry-based proteomics identify novel serum osteoarthritis biomarkers. *Arthritis Res. Ther.* **24**, 120. doi:10.1186/s13075-022-02801-1

Tian, X., Irannejad, R., Bowman, S. L., Du, Y., Puthenveedu, M. A., Von Zastrow, M. and Benovic, J. L. (2016). The α-arrestin ARRDC3 regulates the endosomal residence time and intracellular signaling of the β2-adrenergic receptor. *J. Biol. Chem.* **291**, 14510-14525. doi:10.1074/jbc.M116.716589

Uhrin, P., Dewerchin, M., Hilpert, M., Chrenek, P., Schöfer, C., Zechmeister-Machhart, M., Krönke, G., Vales, A., Carmeliet, P., Binder, B. R. et al. (2000). Disruption of the protein C inhibitor gene results in impaired spermatogenesis and male infertility. *J. Clin. Invest.* **106**, 1531-1539. doi:10.1172/JCI10768

Van Ooijen, M. P., Jong, V. L., Eijkemans, M. J. C., Heck, A. J. R., Andeweg, A. C., Binai, N. A. and Van Den Ham, H. J. (2018). Identification of differentially expressed peptides in high-throughput proteomics data. *Brief. Bioinform.* **19**, 971-981. doi:10.1093/bib/bbx031

Wu, B., Gao, H., Liu, C. and Li, W. (2020). The coupling apparatus of the sperm head and tail†. *Biol. Reprod.* **102**, 988-998. doi:10.1093/biolre/ioaa016

Yeh, C. H., Kuo, P. L., Wang, Y. Y., Wu, Y. Y., Chen, M. F., Lin, D. Y., Lai, T. H., Chiang, H. S. and Lin, Y. H. (2015). SEPT12/SPAG4/LAMINB1 complexes are required for maintaining the integrity of the nuclear envelope in postmeiotic male germ cells. *PLoS One* **10**, e0120722.

Yuan, S., Stratton, C. J., Bao, J., Zheng, H., Bhetwal, B. P., Yanagimachi, R. and Yan, W. (2015). Spata6 is required for normal assembly of the sperm connecting piece and tight head-tail conjunction. *Proc. Natl. Acad. Sci. USA* **112**, E430-E439.

Yue, F., Cheng, Y., Breschi, A., Vierstra, J., Wu, W., Ryba, T., Sandstrom, R., Ma, Z., Davis, C., Pope, B. D. et al. (2014). A comparative encyclopedia of DNA elements in the mouse genome. *Nature* **515**, 355-364. doi:10.1038/nature13992

Zbieralski, K. and Wawrzycka, D. (2022). α-arrestins and their functions: from yeast to human health. *Int. J. Mol. Sci.* **23**, 4988. doi:10.3390/ijms23094988

Zhang, Y., Liu, C., Wu, B., Li, L., Li, W. and Yuan, L. (2021a). The missing linker between SUN5 and PMFBP1 in sperm head-tail coupling apparatus. *Nat. Commun.* **12**, 4926. doi:10.1038/s41467-021-25227-w

Zhang, Y., Yang, L., Huang, L., Liu, G., Nie, X., Zhang, X. and Xing, X. (2021b). SUN5 interacting with Nesprin3 plays an essential role in sperm head-to-tail linkage: research on Sun5 gene knockout mice. *Front. Cell Dev. Biol.* **9**, 684826. doi:10.3389/fcell.2021.684826

Zhang, Z., Zhou, H., Deng, X., Zhang, R., Qu, R., Mu, J., Liu, R., Zeng, Y., Chen, B., Wang, L. et al. (2023). IQUB deficiency causes male infertility by affecting the activity of p-ERK1/2/RSPH3. *Hum. Reprod.* **38**, 168-179. doi:10.1093/humrep/deac244

Zhu, F., Liu, C., Wang, F., Yang, X., Zhang, J., Wu, H., Zhang, Z., He, X., Zhang, Z., Zhou, P. et al. (2018). Mutations in PMFBP1 cause acephalic spermatozoa syndrome. *Am. J. Hum. Genet.* **103**, 188-199. doi:10.1016/j.ajhg.2018.06.010